


PAPER

[View Article Online](#)
[View Journal](#) | [View Issue](#)Cite this: *Dalton Trans.*, 2021, **50**,
4300Development of sterically hindered siloxide-
functionalized polyoxotungstates for the
complexation of 5d-metals†Thomas Auvray,  Olaf Nachtigall,  William W. Brennessel,  William D. Jones 
and Ellen M. Matson *

In this study, we extend the family of organosilyl-functionalized trivacant Keggin polyoxotungstates, $[\text{PW}_9\text{O}_{34}(\text{RSiOH})_3]^{3-}$ ($\text{R} = {}^n\text{Pr}$, ${}^i\text{Pr}$, ${}^t\text{Bu}$), through the introduction of bulky aryl and aliphatic silanol substituents, namely phenyl, cyclohexyl and biphenyl. This work was performed in order to study the impact of these large functional groups on the accessibility of the well-defined tridentate coordination site. Coordination of hafnium to these type II hybrid polyoxotungstates was conducted in order to study the ability of the bulkier ligand pockets to support larger cations in comparison to those previously reported (e.g. Ti^{4+} , V^{3+} , V^{5+} , Ge^{4+}). Increased steric hindrance around the coordination site from the biphenyl groups resulted in much longer reaction times for the complexation reaction compared to the other functional groups used, but the impact of our design toward stabilizing reactive species proved limited, as all complexes easily undergo hydrolysis of the $\text{Hf}-\text{O}^t\text{Bu}$ bond in the presence of water. Electrochemical investigations of the ligands and hafnium complexes reveal that the redox events centered on the polyoxotungstate core can be tuned by varying the substituents on the silyl fragment, and exhibit a cathodic shift after coordination of the redox inactive tetravalent cation.

Received 25th January 2021,
Accepted 27th February 2021

DOI: 10.1039/d1dt00256b

rsc.li/dalton

Introduction

Surface organometallic chemistry is a powerful strategy for the development of heterogeneous catalysts exhibiting well-defined active sites. By approaching the surface of the supporting materials as a polydentate ligand, molecular precursors can be used to prepare catalytic materials with active sites whose coordination environment can be explicitly determined.^{1–3} A specific toolbox of characterization methods has been developed to explore these systems in order to gain insights regarding the nature of the surface active sites and establish structure–activity relationships to further inform catalyst design.⁴ However, despite advances in the characterization techniques available for these heterogeneous systems, the use of molecular models remains an efficient approach to further improve our understanding of the reaction mechanisms during heterogeneous catalysis. This approach takes

advantage of well-established homogenous chemistry to synthetically tune the coordination environment, and provides access to complementary analytical methods (such as solution NMR or single crystal X-ray diffraction). In this context, discrete assemblies with well-defined coordination sites, such as polyhedral oligomeric silsesquioxanes, have been shown to be suitable models for their bulk congeners.^{5,6}

Polyoxometalates (POMs) are an attractive class of compounds for the development of model systems for both metal oxide surfaces and single-atom active sites.^{7,8} To better understand the reactivity of organometallic compounds supported by metal oxide surfaces, derivatives of POMs appended to transition metal complexes have been extensively studied. POMs can be attached to pre-generated organometallic units *via* salt metathesis reactions, resulting in the formation of metal–oxygen bonds to the terminal and/or bridging O atoms of the POM.⁹ The metal–oxygen bonds in these assemblies are usually quite labile due to the weak basicity of the surface O atoms of POMs, resulting in poor electrostatic interactions that are easily disrupted by coordinating solvents or other nucleophiles.^{10,11} To circumvent these challenges, researchers have taken advantage of an attractive feature of POMs, the ability to generate lacunary assemblies. Lacunary POMs are prepared either by exposure of plenary motifs to base, where one or more of the constitutive metal centers is removed,

Department of Chemistry, University of Rochester, Rochester, NY, 14627, USA.

E-mail: matson@chem.rochester.edu

†Electronic supplementary information (ESI) available: ${}^1\text{H}$ NMR analysis and electrochemical data for all compounds, crystallographic parameters for ligand **4**, complex **6** and hydrolysed variant of complex **7**. CCDC 2058486–2058488. For ESI and crystallographic data in CIF or other electronic format see DOI: 10.1039/d1dt00256b

leaving well-defined vacant coordination sites with highly reactive, nucleophilic surface oxygen atoms, or directly from the starting metalates under strict pH control.¹² This lacuna can then be filled with another metal,^{13–16} creating heterometal functionalized POMs that can be used to model point defects at metal oxide surfaces.^{17,18} Alternatively, researchers have used lacunary POMs as precursors to prepare so called “type II” hybrid organic–inorganic assemblies with covalent interaction between the constitutive units. To this end, a rich library of organofunctionalization strategies has been reported, taking advantage of the nucleophilic oxygen atoms of the vacant sites;^{19,20} examples include alkoxide,^{21,22} siloxide,^{23,24} organophosphonyl^{25,26} or organotin derivatives.²⁷ Interestingly, the formation of these hybrid polyoxometalate structures not only allows introduction of additional functionality/dimensionality to the newly formed hybrid, but also the ability to tune the physicochemical properties of the POM unit.^{28,29}

Among these organofunctionalized species, organosilyl-functionalized, trivacant Keggin polyoxotungstates have been successfully employed by Guillemot and co-workers as models for monometallic titanium or vanadium active sites on silicon oxide surfaces.^{30–33} These hybrid compounds were initially prepared by Mazeaud *et al.*, who explored the reactivity of trichlorosilanes with the trilacunary cluster $[\text{EW}_9\text{O}_{34}]^{9-}$ (E = P, Si). The authors showed that using *tert*-butyltrichlorosilane, they could isolate an organofunctionalized species, $[\text{PW}_9\text{O}_{34}(\text{tBuSiOH})_3]^{3-}$ (Fig. 1), with a well-defined 3-fold symmetrical pocket generated by the insertion of three silanol fragments.²³ Isolation of that open species is favored by the steric hindrance of the *tert*-butyl groups, while the use of trichlorosilanes with decreased steric bulk in the aliphatic functional group manifested in capped structures, where a fourth equivalent of trichlorosilane

reacted with the three silanol groups to generate the cluster $[\text{PW}_9\text{O}_{34}(\text{RSiO})_3(\text{SiR})]^{3-}$ (R = H, Me, Et, *n*Bu, *etc.*). Interestingly, Guillemot and co-workers recently used a combined experimental-theoretical approach to prepare species with reduced steric hindrance.³³ Following metalation of these clusters with titanium, complexes were generated with enhanced catalytic activity for alkene epoxidation, allowing their research team to develop a reliable model for the tetrahedral defective open-lattice $[(\text{Si}-\text{O})_3\text{Ti}(\text{OH})]$ sites that are present in crystalline microporous Ti-silicalites (such as TS-1).

Here, we report our efforts focused on the introduction of bulky organosilanol substituents to the surface of the trilacunary assembly, in order to reduce the accessibility to the metal site and potentially stabilize reactive adducts of 2nd and 3rd row transition metal ions. Our studies have focused on the installation of Hf(IV) ions in the pocket of these organofunctionalized polyoxotungstates; while this transition metal is established to have similar reactivity in comparison to Ti(IV) ions, its larger effective ionic radius in tetracoordinated environments (0.58 Å) compared to Ti(IV) (0.42 Å) led our team to hypothesize that bulkier ligands would increase the stability of Hf-substituted trisilanol derivatives of the trilacunary polyoxotungstate.³⁴ The complexation reactions appeared to proceed on different time scales depending on the steric hindrance around the silanol-delineated coordination site, with installation of Hf on the biphenyl-functionalized ligand being the slowest. This observation confirms our hypothesis regarding reduced accessibility of the cavity in the presence of sterically encumbered functional groups. Electrochemical investigations of the prepared ligands revealed that the nature of the substituent of the organosilyl unit modifies the redox potential of the polyoxotungstate unit. Coordination of hafnium to these species translates to a cathodic shift of all redox events, allowing one to finely tune the redox profile of these hybrid assemblies by stepwise modification.

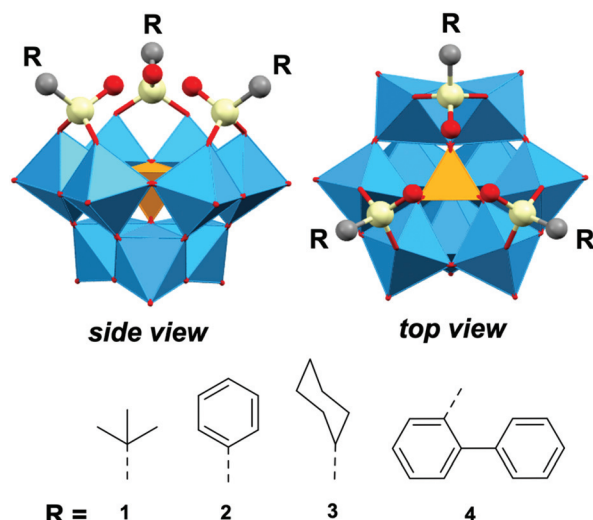


Fig. 1 Siloxide-functionalized, trilacunary polyoxotungstate clusters, $[\text{PW}_9\text{O}_{34}(\text{RSiOH})_3]^{3-}$. “R” functional groups highlighted on the bottom of the figure show the sterically bulky variants of the polyoxotungstate motif studied in this work. Grey sphere: C; red sphere: O; pale yellow sphere: Si; cyan polyhedron: W; orange polyhedron: P.

Results and discussion

Synthesis of organosilyl-functionalized, trilacunary polyoxotungstates

The targeted silanol decorated clusters (Fig. 1) were obtained by reaction between trichlorosilane derivatives (RSiCl_3 ; R = *t*Bu, Ph, Cy, PhPh) and the trilacunary Keggin anion $[\text{PW}_9\text{O}_{34}]^{9-}$ (synthetic details provided in the Experimental section). First, the trilacunary cluster, $[\text{PW}_9\text{O}_{34}]^{9-}$, was isolated as its potassium salt by controlled hydrolysis of the monolacunary species, $[\text{PW}_{11}\text{O}_{39}]^{7-}$, as described by Contant.³⁵ It was then reacted with the suitable trichlorosilane derivatives using the procedure established by Mazeaud *et al.*²³ These authors showed that installation of the organosilyl moieties requires the presence of small amounts of water to hydrolyze the trichlorosilanes into the corresponding silanetriols which then react with the lacunary cluster under the employed heterogeneous conditions.²³ Similar reaction pathways are proposed to operate in the case of these sterically encumbered trichlorosilanes. While

the *tert*-butyl, phenyl and cyclohexyl-trichlorosilanes are commercially available, [1,1'-biphenyl]-2-yltrichlorosilane was prepared using a modified procedure through preparation of the organolithium intermediate, LiR, as described for other aryltrichlorosilanes, and its subsequent addition to tetrachlorosilane.³⁶ Tetrahexylammonium bromide (THABr) was used as a phase-transfer reagent, as described by Guillemot and co-workers,^{30,31} and provides tetrahexylammonium counter-cations to the final products in order to extend their solubility to a wide range of organic solvents, a common strategy in polyoxometalate chemistry.³⁷

The successful functionalization of $[\text{PW}_9\text{O}_{34}]^{9-}$ was confirmed by multinuclear magnetic resonance spectroscopy (^1H , $^{31}\text{P}\{^1\text{H}\}$), electrospray ionization mass spectrometry (ESI-MS), and elemental analysis, as well as structural analysis by single crystal X-ray diffraction (*vide infra*). The ^1H NMR spectra of the functionalized species 1–4 (Fig. S1–S4†) present the expected resonances for the three THA counter-cations and that of the substituent on the silanol units. The silanol protons are observed as a sharp singlet between 4.7 and 5.9 ppm after thorough drying of the compounds at 210 °C under vacuum, consistent with observations made by Guillemot and co-workers.²⁴ In the case of the cyclohexyl derivative 3 ($\text{THA}_3[\text{PW}_9\text{O}_{34}(\text{CySiOH})_3]$), significant overlap between the cyclohexyl and THA resonances is observed. Their $^{31}\text{P}\{^1\text{H}\}$ NMR spectra present a sharp singlet between –15.8 and –16 ppm. All compounds were observed as tri-anionic species by ESI-MS. These organofunctionalized clusters are readily dissolved in acetonitrile and THF, with complex 3 ($\text{THA}_3[\text{PW}_9\text{O}_{34}(\text{CySiOH})_3]$), bearing cyclohexyl substituents, being the least soluble amongst the four compounds isolated. This behavior highlights the possibility of tuning the solubility of the hybrid assemblies through the variation of the substituent of the organosilyl fragment.

Crystals of ligand 4 ($\text{THA}_3[\text{PW}_9\text{O}_{34}(\text{PhPhSiOH})_3]$) suitable for X-ray diffraction were obtained by layering methanol onto a solution of the cluster in acetonitrile. Two individual clusters are found in the asymmetric unit, along with the six expected counter-cations which are severely disordered (see ESI† for additional refinement details). Initial comparison of the bond lengths with the structure previously reported for 1 ($\text{THA}_3[\text{PW}_9\text{O}_{34}(\text{tBuSiOH})_3]$)²³ shows that replacing the *tert*-butyl substituents by biphenyl groups does not result in significant change in the structural parameters of the cavity. As such, we will not discuss structural parameters of this compound in detail as the severe disorder in the crystal structure results in low precision on the bonds within the model. Interestingly, the threefold symmetry of the cluster observed in solution, due to the free rotation of the substituents, is not retained in the solid state. Both functionalized species in the asymmetric unit adopt the configuration presented in Fig. 2, with two of the biphenyls pointing upward and one aligned with the cluster framework. This orientation of the biphenyl moieties results in a less accessible coordination site, with two sides of the triangle delineated by silanol units being obstructed by one of the terminal phenyl rings. This obser-

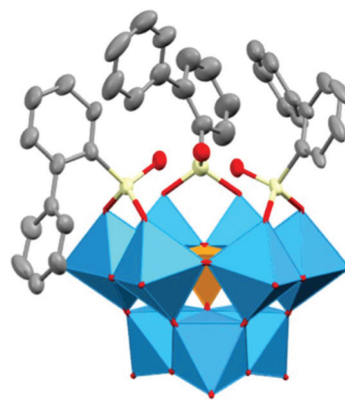


Fig. 2 Combined ellipsoid (30% probability) and polyhedral representation of the ligand 4 ($\text{THA}_3[\text{PW}_9\text{O}_{34}(\text{PhPhSiOH})_3]$). Counter-cations and hydrogen atoms have been omitted for clarity. Grey: C; red: O; pale yellow: Si; cyan polyhedron: W; orange polyhedron: P.

vation confirms our initial hypothesis that using bulkier substituents reduces the accessibility of the coordination pocket in comparison to the previously reported *tert*-butyl derivative (see Fig. S14†). Based on the successful design offered by an *ortho*-substituted phenyl unit, we attempted to introduce the bulkier mesityl moieties (mesityl = 2,4,6-trimethylphenyl), unfortunately without success, indicating a possible limit to the steric hindrance compatible with the cavity.

Introduction of organic functional groups on POMs is known to impact their electronic properties.^{28,38} For example, in their study of the impact of functionalization of the monolacunary Dawson polyoxotungstate cluster, $[\text{P}_2\text{W}_{17}\text{O}_{61}]^{10-}$, Mayer, Odobel and co-workers showed that introduction of either organosilyl or organophosphonyl groups results in more clearly resolved redox events in electrochemical measurements than observed for the parent plenary anion, $[\text{P}_2\text{W}_{18}\text{O}_{62}]^{6-}$. The two functionalization strategies have, however, opposite impacts on the redox events, with an anodic shift for the organophosphonyl species, $[\text{P}_2\text{W}_{17}\text{O}_{61}(\text{PhPO})_2]^{6-}$ and a cathodic shift after installation of organosilyl moieties in the case of $[\text{P}_2\text{W}_{17}\text{O}_{62}(\text{PhSi})_2]^{6-}$.²⁹ This difference in behavior was explained by the relative electron withdrawing nature of the phenylphosphonyl and phenylsiloxide groups, the latter being a weaker electrophile. Subsequent studies by Proust and co-workers on organosilyl functionalized monolacunary Keggin polyoxotungstate clusters bearing alkyl or aryl substituents showed little impact of the nature of these substituents on the electrochemical profile of the assemblies,^{39,40} presumably due to the limited electronic conjugation across the siloxane linker.⁴¹ These reports are in contrast with other systems such as the Lindqvist hexavanadate cluster, $[\text{V}_6\text{O}_{13}\{(\text{OCH}_2)_3\text{CR}\}_2]^{2-}$, studied by Zubieta and coworkers.⁴² In this case, the authors showed that changing the nature of the substituent R on the triol moiety allows tuning of the redox properties of the assemblies over a range of 600 mV, with a direct correlation between reduction potential and Hammett constant of the substituents.

We thus investigated the impact of our functionalization efforts with both alkyl and aryl substituents on the electrochemical properties of the polyoxotungstate core in anhydrous acetonitrile. The cyclic voltammograms (CVs) of compounds 1–4 are presented in Fig. 3 while the potential values are reported in Table 1 (additional data available in the ESI, Fig. S18–S21†). All four trisilanol decorated Keggin anions exhibit three successive reversible one-electron reductions (note, compounds 1, 2, and 4 possess an additional irreversible event located ~ -2.3 V). The redox potentials observed for compound 1 ($\text{THA}_3[\text{PW}_9\text{O}_{34}(\text{tBuSiOH})_3]$) match those previously reported by Proust and co-workers.⁴³ Interestingly, noticeable shifts in reduction potentials are observed between compounds 1 ($\text{THA}_3[\text{PW}_9\text{O}_{34}(\text{tBuSiOH})_3]$) and 2 ($\text{THA}_3[\text{PW}_9\text{O}_{34}(\text{PhSiOH})_3]$); we attribute these changes in reduction potential to the electron withdrawing character of the phenyl substituents bound to the surface of the cluster in the case of com-

pound 2. Comparing the two aryl-substituted species, 2 ($\text{THA}_3[\text{PW}_9\text{O}_{34}(\text{PhSiOH})_3]$) and 4 ($\text{THA}_3[\text{PW}_9\text{O}_{34}(\text{PhPhSiOH})_3]$), a significant shift towards more negative reduction potentials is observed for the biphenyl derivative 4, reflecting the more electron rich character of that substituent compared to the phenyl in 2. The trend in reduction potential is: $2 \gg 4 > 3 \approx 1$, with both aryl-substituted species being easier to reduce than their aliphatic counterparts. This trend agrees with the relative electron donating ability of the organosilyl groups used in the present study.

Complexation of hafnium

Adapting the complexation procedure reported for the Ti-analogs,³⁰ reaction of the thoroughly dried hybrid polyoxotungstate clusters, species 1–4, with $\text{Hf}(\text{O}^t\text{Bu})_4$ led to quantitative formation of the desired hafnium complexes 5–8, as indicated by product analysis with ^1H and $^{31}\text{P}\{^1\text{H}\}$ NMR spectroscopies (the evolution of the ^1H and $^{31}\text{P}\{^1\text{H}\}$ NMR spectra over time is presented in Fig. 4 for the reaction of 4 ($\text{THA}_3[\text{PW}_9\text{O}_{34}(\text{PhPhSiOH})_3]$) with $\text{Hf}(\text{O}^t\text{Bu})_4$). Products were isolated from the crude reaction mixture through precipitation/crystallization from THF solution by addition/slow diffusion of Et_2O .

When attempting to follow the complexation reaction by ^1H and $^{31}\text{P}\{^1\text{H}\}$ NMR spectroscopy, we observed complete reaction in the case of ligands 1–3 by the time the tube was inserted in the instrument (<5 min). In contrast, in the case of the biphenyl-equipped ligand, compound 4 ($\text{THA}_3[\text{PW}_9\text{O}_{34}(\text{PhPhSiOH})_3]$), complexation of Hf to the siloxide-functionalized polyoxotungstate occurred over the course of 24 h. No intermediate species is observed as the reaction proceeds. Conversion from 4 to 8 also leads to the formation of *tert*-butanol, as clearly observed in Fig. 4a. This difference in behavior for the biphenyl-decorated cluster confirms our hypothesis that bulkier substituent can block access to the coordination site. Indeed, the crystal structure of ligand 4 showed that the biphenyl substituents can partially block the cavity by capping the sides of the threefold symmetrical coordination site, depending on their orientation. In addition, the three biphenyl moieties appear to be moving around the cavity in

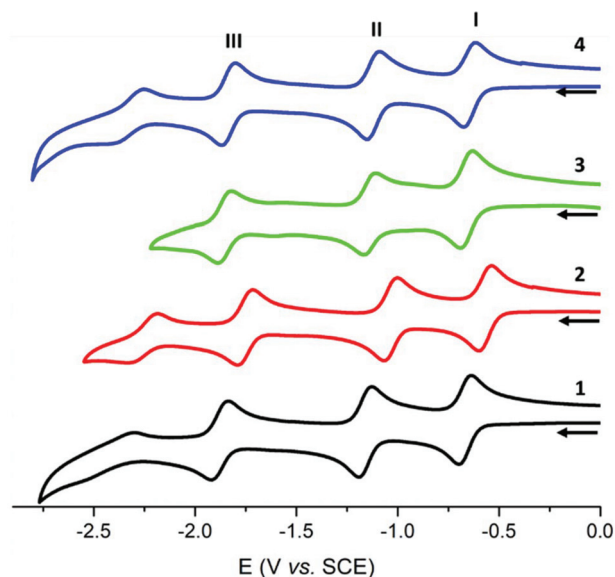


Fig. 3 Cyclic voltammograms of ligands 1 (black), 2 (red), 3 (green), and 4 (blue) collected in dry, deaerated acetonitrile with 0.1 M $[\text{tBu}_4\text{N}][\text{PF}_6]$ as the supporting electrolyte.

Table 1 Electrochemical parameters for ligands 1–4 determined by cyclic voltammetry in dry deaerated acetonitrile, using $[\text{tBu}_4\text{N}][\text{PF}_6]$ as supporting electrolyte and ferrocene as internal reference

Compound	Process	E_{pa} V vs. SCE	E_{pc} V vs. SCE	$E_{1/2}$ V vs. SCE	ΔE_{mv}
1 $\text{THA}_3[\text{PW}_9\text{O}_{34}(\text{tBuSiOH})_3]$	I	−0.638	−0.699	−0.669	61
	II	−1.129	−1.191	−1.160	62
	III	−1.838	−1.921	−1.880	83
2 $\text{THA}_3[\text{PW}_9\text{O}_{34}(\text{PhSiOH})_3]$	I	−0.538	−0.598	−0.568	60
	II	−1.001	−1.067	−1.034	66
	III	−1.717	−1.790	−1.754	73
3 $\text{THA}_3[\text{PW}_9\text{O}_{34}(\text{CySiOH})_3]$	I	−0.632	−0.691	−0.662	59
	II	−1.107	−1.169	−1.138	62
	III	−1.821	−1.888	−1.855	67
4 $\text{THA}_3[\text{PW}_9\text{O}_{34}(\text{PhPhSiOH})_3]$	I	−0.616	−0.675	−0.646	59
	II	−1.090	−1.151	−1.121	62
	III	−1.802	−1.869	−1.836	67

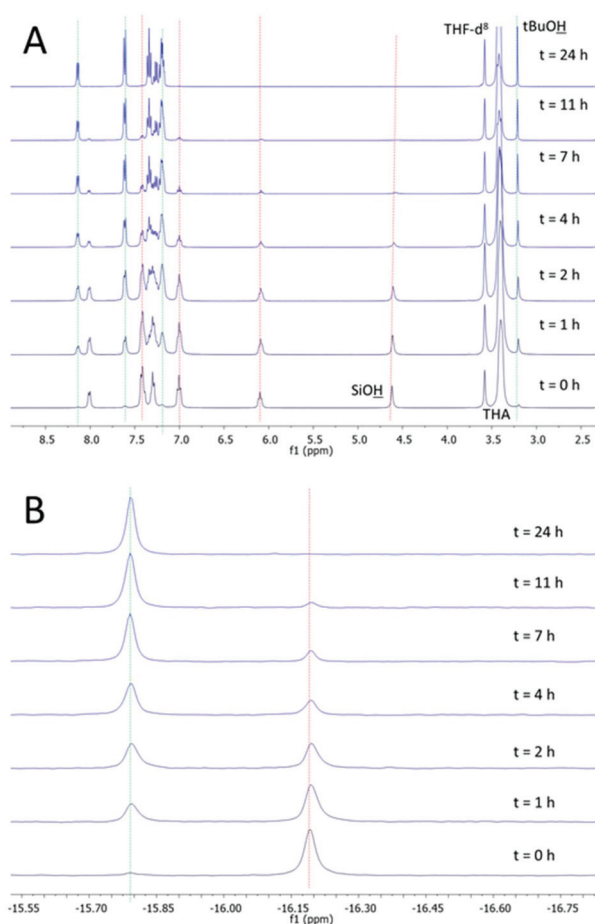


Fig. 4 Monitoring of complexation of hafnium via the reaction of $\text{Hf}(\text{O}^t\text{Bu})_4$ and compound **4** ($\text{THA}_3[\text{PW}_9\text{O}_{34}(\text{PhPhSiOH})_3]$) in THF-d_8 by (A) ^1H and (B) $^{31}\text{P}\{^1\text{H}\}$ NMR spectroscopy.

solution, as confirmed by their protons being equivalent in the NMR spectra. This dynamic behavior results in a less accessible cavity and drastically affects the kinetics of $\text{Hf}(\text{O}^t\text{Bu})_4$ protonolysis.

The successful complexation of hafnium to the organofunctionalized species was confirmed by multinuclear magnetic resonance spectroscopy (^1H , $^{31}\text{P}\{^1\text{H}\}$) and elemental analysis, as well as structural analysis by X-ray diffraction (*vide infra*). In all cases, ^1H NMR spectroscopy shows that reaction with $\text{Hf}(\text{O}^t\text{Bu})_4$ led to the disappearance of the resonance attributed to the silanol groups and apparition of a resonance corresponding to the *tert*-butoxide ligand (see Fig. S5–S8†). The alkyl/aryl substituents on the siloxide groups are somewhat affected by the coordination of the hafnium cation, leading overall to small shifts in their respective resonances. In all cases, the three siloxide units appear equivalent, indicating that the threefold symmetry is conserved, in solution, after complexation. The $^{31}\text{P}\{^1\text{H}\}$ NMR spectra present one sharp singlet for the central phosphorus atom, as observed for the corresponding ligands, confirming the formation of a single species in all cases. These resonances appear between -15.7

and -16.4 ppm, corresponding to a slightly more shielded phosphorus atom in the case of complexes **5**–**7**, in agreement with the slight increase in local electron density after deprotonation of the silanol. In the case of compound **8** ($\text{THA}_3[\text{PW}_9\text{O}_{34}(\text{PhPhSiO})_3\text{Hf}(\text{O}^t\text{Bu})]$), however, the $^{31}\text{P}\{^1\text{H}\}$ resonance is shifted downfield compared to the free ligand **4** ($\text{THA}_3[\text{PW}_9\text{O}_{34}(\text{PhPhSiOH})_3]$). This could be attributed to the loss, after complexation, of the additional shielding provided by the external phenyl ring covering the free coordination pocket in the ligand, as discussed previously. Elemental analysis confirmed the purity of the compounds, though partial hydrolysis was observed in the case of complex **7**, despite our effort to minimize its exposure to moisture.

Crystals suitable for X-ray diffraction were obtained by slow diffusion of diethyl ether into a concentrated solution of complex **6** ($\text{THA}_3[\text{PW}_9\text{O}_{34}(\text{PhSiO})_3\text{Hf}(\text{O}^t\text{Bu})]$) in deuterated THF. Interestingly, the structure, shown in Fig. 5, revealed the presence of two THF- d_8 solvent molecules coordinated to the Hf center in addition of the expected *tert*-butoxide ligand, resulting in an hexacoordinated metal center instead of the tetra-coordinated species obtained by Guillemot and co-workers for the Ti-analog equipped with *tert*-butyl substituents.³⁰ This increased coordination number is not unexpected for a third row transition metal such as hafnium but results in the loss of the threefold symmetry observed in the NMR spectrum of complex **6** ($\text{THA}_3[\text{PW}_9\text{O}_{34}(\text{PhSiO})_3\text{Hf}(\text{O}^t\text{Bu})]$) with the three phenyl groups being equivalent. The slightly lower steric hindrance from the phenyl substituent, due to its planarity, might contribute to the ability to accommodate additional ligand(s) in the coordination site. We were however unable to obtain the structure of the other complexes to confirm if this solvent adduct is specific to the phenyl derivative. In addition, the expected longer Si–O–M bonds were observed in the crystal structure of the Hf complex compare to those of the Ti species (average of 1.99 Å vs. 1.81 Å, respectively), resulting in a metal center further away from the silicon atoms, reducing the impact of variation in the steric hindrance of the substituting groups.

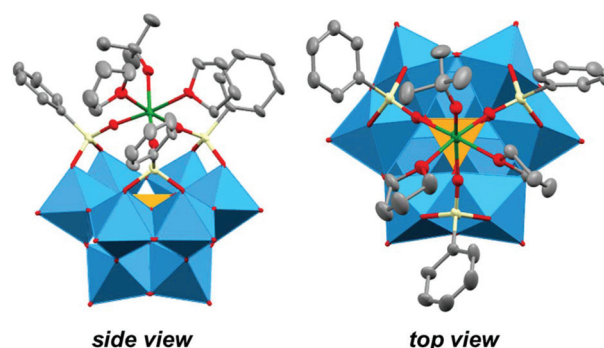


Fig. 5 Combined ellipsoid (30% probability) and polyhedral representation of the THF-adduct of complex **6** ($\text{THA}_3[\text{PW}_9\text{O}_{34}(\text{PhSiO})_3\text{Hf}(\text{O}^t\text{Bu})](\text{THF})_2$). Counter-cations, co-crystallized solvent molecules and hydrogen atoms are omitted for clarity. Grey: C; red: O; pale yellow: Si; green: Hf; cyan polyhedron: W; orange polyhedron: P.

The electrochemical profiles of the hafnium complexes were studied by cyclic voltammetry in dry deaerated acetonitrile. The CVs are presented in Fig. 6 (and Fig. S22–S25†) and the potentials reported in Table 2. While the ligands 1–4 possessed three reversible redox events, the complexes 5–8 only present two events in the same electrochemical window (a third event is observed in the case of complex 5, $\text{THA}_3[\text{PW}_9\text{O}_{34}(\text{tBuSiO})_3\text{Hf}(\text{O}^t\text{Bu})]$). Furthermore, these events are cathodically shifted by approximately 200 mV and appear quasi-reversible, based on the large difference between anodic and cathodic peaks. Interestingly, the trend in ease of reduction observed for the ligands is retained, with complex 6, based on ligand 2 ($\text{THA}_3[\text{PW}_9\text{O}_{34}(\text{PhSiOH})_3]$) bearing phenyl substituents, being easier to reduce by 80 mV compared to the alkyl substituted complexes, 5 and 7, and by 60 mV compared to complex 8, bearing the biphenyl groups.

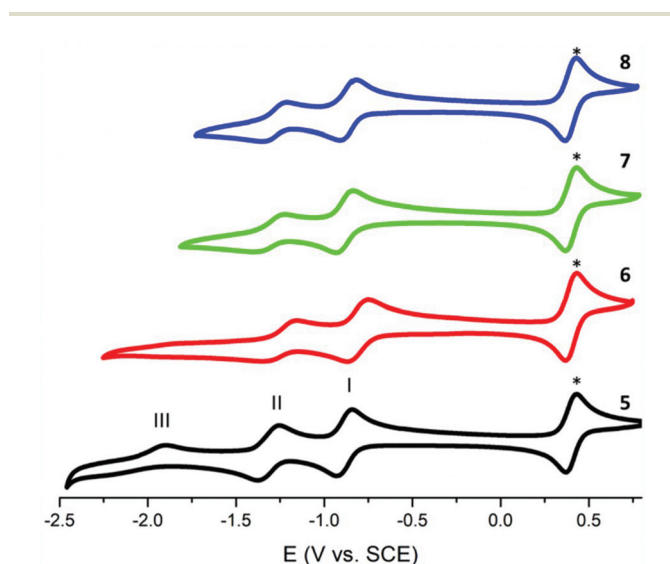


Fig. 6 Cyclic voltammograms of the Hf complexes ($\text{THA}_3[\text{PW}_9\text{O}_{34}(\text{RSiO})_3\text{Hf}(\text{O}^t\text{Bu})]$) 5 (black, R: $t\text{Bu}$), 6 (red, R: Ph), 7 (green, R: Cy), and 8 (blue, R: PhPh) collected in dry, deaerated acetonitrile with 0.1 M $[\text{tBu}_4\text{N}][\text{PF}_6]$ as the supporting electrolyte and ferrocene as internal reference (*).

Table 2 Electrochemical parameters for complexes 5–8 determined by cyclic voltammetry in dry deaerated acetonitrile, using $[\text{tBu}_4\text{N}][\text{PF}_6]$ as supporting electrolyte and ferrocene as internal reference

Compound	Process	E_{pa} V vs. SCE	E_{pc} V vs. SCE	$E_{1/2}$ V vs. SCE	ΔE_{mV}
5	I	−0.841	−0.930	−0.886	89
	II	−1.256	−1.377	−1.317	121
	III	−1.899	−2.208	≈ -2	309
6	I	−0.748	−0.868	−0.808	120
	II	−1.154	−1.353	−1.254	199
7	I	−0.836	−0.933	−0.885	97
	II	−1.221	−1.402	−1.312	181
8	I	−0.816	−0.911	−0.864	95
	II	−1.210	−1.353	−1.282	143

A similar cathodic shift for the redox events involving the polyoxotungstate core was previously observed for the Ge-substituted assembly reported by Proust and co-workers ($\Delta E_{1/2} = 120 \text{ mV}$).⁴³ These cathodic shifts are tentatively attributed to the presence of the three additional negative charges from the three siloxide units localized within the coordination pocket and only partially balanced by the cation introduced, leading to an overall increase in charge of the polyoxotungstate core.⁴⁴ In addition, the reversibility of the redox events observed for the ligand was retained in the case of the Ge derivatives, unlike what is observed for our Hf complexes. This includes complex 5 bearing the same *tert*-butyl substituents. Based on the reduced current observed in all cases for the second reduction compared to that of the first event, we propose this loss of reversibility to arise from important structural rearrangement after reduction, such as de-coordination of solvent molecule(s) from the Hf center as observed in the crystal structure of complex 6 discussed above.

In contrast to our observations, Newton and coworkers observed anodic shifts of the reduction processes after complexation in their study of organophosphonyl derivatives of the monolacunary Dawson polyoxotungstate cluster, $[\text{P}_2\text{W}_{17}\text{O}_{61}(\text{P}(\text{O})\text{C}_6\text{H}_4\text{CO}_2\text{H})_2]^{6-}$.^{45,46} However, the inverse shift of the reduction potentials can be explained using the same reasoning as for our system. Binding of the divalent cation (*i.e.* Zn^{2+} , Co^{2+} or Mn^{2+}) to the neutral phosphonyl ligand results in a decrease of the negative charge of the polyoxotungstate core, leading to its easier reduction.

Reactivity of water with the hafnium functionalized assemblies

In order to determine the impact of varied steric hindrance around the coordinated pocket on the stability of the coordinated reactive species, we wanted to probe the stability of the Hf–O^{*t*}Bu bond towards hydrolysis. However, all four Hf complexes, compounds 5–8, appear to easily undergo hydrolysis of the Hf–O^{*t*}Bu bond, both in the solid state and in solution. This decomposition occurred despite storage of the complexes in the glovebox to limit their exposure to moisture. The hydrolysis can easily be monitored by ^1H and $^{31}\text{P}\{^1\text{H}\}$ NMR spectroscopies (Fig. S9–S12†). It leads to the appearance of resonances corresponding to free *tert*-butanol and an additional broad singlet between 3.7 and 4.7 ppm integrating to one proton. This new resonance is tentatively attributed to the hydroxide ligand formed as a result of hydrolysis. The resonances of the alkyl or aryl substituents are also slightly shifted but no general trend is observed, and the three substituents remain equivalent. The $^{31}\text{P}\{^1\text{H}\}$ NMR spectra present a small upfield shift of the singlet for the central phosphorus atom, indicating the existence of a single species in acetonitrile. ESI-MS analysis in acetonitrile confirmed the formation of the hydroxide species, observed as the triply charged anion $[\text{PW}_9\text{O}_{34}(\text{RSiO})_3\text{Hf}(\text{OH})]^{3-}$. A similar species was identified by Guillemot and co-workers who observed by NMR spectroscopy the formation of $[\text{PW}_9\text{O}_{34}(\text{tBuSiO})_3\text{Ti}(\text{OH})]^{3-}$ and confirmed it to be a monomeric species based on DOSY NMR.³⁰

The equilibrium between monomeric and dimeric species is a recurring point of discussion in previous reports of Hf-functionalized POMs, in particular in the context of their use as catalysts for various organic transformations (e.g. Mannich-type additions,⁴⁷ Mukaiyama aldol reaction⁴⁸ or amide bond formation⁴⁹). This equilibrium has been shown to be highly condition dependent; in particular, it is clearly affected by the solvent used, as recently demonstrated by Parac-Vogt and co-workers.⁵⁰ Interestingly, while NMR and MS analysis pointed to the formation of monomeric species, crystals suitable for X-ray diffraction were obtained for the hydrolyzed form of complexes **5** and **7** revealing the existence of dimeric complexes. In the case of the hydrolyzed derivative of **5**, the dataset was incomplete, resulting only in a preliminary structure. We will thus limit our discussion of this structure to its connectivity. In this symmetrical dimeric structure, two Hf cations are supported by two *tert*-butylsiloxide functionalized clusters and bridged by two hydroxo groups (see the corresponding section in the ESI†). The coordination sphere of each Hf cation is potentially completed by water molecule(s) that could not be definitively assigned with the incomplete dataset. On the other hand, crystallization of the product of hydrolysis of complex **7** in “wet” solvents (e.g. using commercially available solvents without taking any additional drying steps) led to the isolation of the compound presented in Fig. 7. It is similar to the preliminary structure obtained for the hydrolyzed form of complex **5**, with a symmetrical dimer based on two Hf cations supported by cyclohexylsiloxide functionalized polyoxotungstate and connected by two bridging hydroxo groups. In the case of the structure of the hydrolyzed variant of complex **7**, water molecules complete the coordination sphere of the metal, resulting in hexacoordinate Hf cations. The nature of the bridging ligand was determined based on charge balance as three tetrahexylammonium ions, though severely disordered, were localized in the asymmetric unit containing one of the Hf-hydroxo bearing polyoxotungstates, as the dimer sits

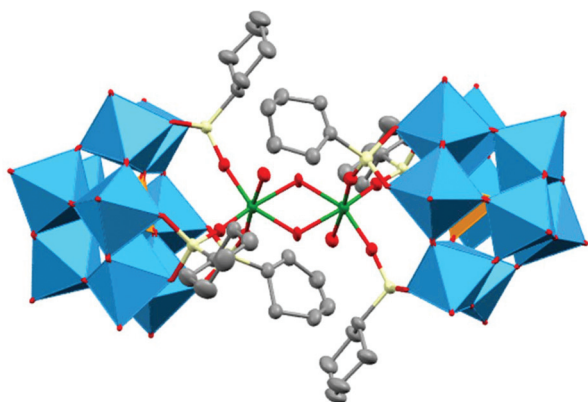


Fig. 7 Combined ellipsoid (30% probability) and polyhedral representation of the hydrolysed form of complex **7**. Counter-cations, co-crystallized solvent molecules and hydrogen atoms are omitted for clarity. Grey: C; red: O; pale yellow: Si; green: Hf; cyan polyhedron: W; orange polyhedron: P.

on an inversion center. Thus, in both cases, we observed once again the trend towards extended coordination number for the Hf cations. The presence of coordinated water molecules in both structures suggests that coordination of oxygenated solvent might play a role in the equilibrium between monomeric and dimeric species.

We next decided to collect the cyclic voltammograms of these hydroxo species to see if a change in the nature of the ligand on the redox inactive cation installed within the coordination pocket had an effect on the electronic properties of the assemblies. The cyclic voltammograms are shown in Fig. S26–S29.† At first look, the general position of each redox event matches the potential determined for freshly prepared complexes, indicating that hydrolysis of the alkoxide ligand does not affect the redox profile of the assemblies, as expected. However, the fact that several overlapping redox events are observed suggests the presence of multiple species in solution. This is in agreement with the fact that these complexes can exist as both monomer and dimer, as discussed above. In fact, the equilibrium between dimer and monomer is likely displaced towards the dimer in the electrochemical conditions because of the higher concentration used (1 mM), especially compared to the concentration used for other analyses, such as ESI-MS. The presence of residual free *tert*-butanol after drying the samples is also a possible explanation, as it has previously been shown to coordinate to Hf even after protonolysis,⁵¹ and could contribute to the reorganization process after reduction mentioned for the alkoxide complexes above.

Conclusion

In this study, we successfully prepared new organosilyl derivatives of the trilacunary Keggin polyoxotungstate, introducing bulkier substituents compared to previous reports. Structural characterization of the biphenyl derivative, **4** ($\text{THA}_3[\text{PW}_9\text{O}_{34}(\text{PhPhSiOH})_3]$), shows that the increased steric hindrance results in lower accessibility of the coordination pocket. This was further confirmed during complexation with an Hf alkoxide precursor, where the reduced accessibility to the silanol sites lead to a much longer reaction time in the case of ligand **4**. This differs from the synthesis of complex **8** ($\text{THA}_3[\text{PW}_9\text{O}_{34}(\text{PhPhSiO})_3\text{Hf}(\text{O}^t\text{Bu})]$), which takes a full day compared to a few minutes for complexes **5**–**7**, with *tert*-butyl, phenyl, and cyclohexyl substituents, respectively.

Electrochemical investigations revealed that varying the nature of the organic substituent allows tuning of the redox properties of the phosphotungstate core in these hybrid assemblies, according to the electron donating/withdrawing properties of the functional groups. Coordination of Hf results, however, in a loss of reversibility for the redox events of the assemblies, along with a cathodic shift of the reduction potentials, presumably due to this large third row transition metal cation being a soft Lewis acid.

Contrary to our initial hypothesis, increased steric hindrance did not prevent hydrolysis of the highly reactive Hf-

O^tBu bond in the presence of a small amount of water, leading to the formation of hydroxo species. Characterization of these hydrolyzed species showed that they can exist as both monomers and hydroxyl-bridged dimers, depending on the conditions, as described for other POM-based Hf-containing assemblies. The presence of accessible coordination sites on the Hf center, occupied by solvent molecules after synthesis, coupled with the tunable environment around the metal center, makes the assemblies reported herein potentially interesting catalysts for Mannich additions or amide bond formations.

Experimental

General considerations

All manipulations were carried out in the absence of water and oxygen either using an argon purged Schlenk line or in a UniLab MBraun inert atmosphere glovebox (N₂). Glassware was oven-dried for a minimum of 4 h and cooled either under positive flow of argon or in an evacuated antechamber prior to use in the drybox. Unless otherwise noted, solvents were dried and deoxygenated on a Glass Contour System (Pure Process Technology, LLC) and stored over activated 3 Å molecular sieves purchased from Fisher Scientific. Tert-butyltrichlorosilane, phenyltrichlorosilane, cyclohexyl-trichlorosilane and hafnium *tert*-butoxide were obtained from commercial sources and used as received. K₉[PW₉O₃₄]·16H₂O was prepared following a published procedure.³⁵

¹H, ¹³C{¹H} and ³¹P{¹H} NMR spectra were recorded on a Bruker DPX-400 MHz spectrometer locked on the signal of deuterated solvents. All chemical shifts were reported relative either to the peak of a residual signal of the deuterated solvents (¹H, ¹³C) or H₃PO₄ (³¹P). CDCl₃ and CD₃CN were purchased from Cambridge Isotope Laboratories, degassed by three freeze–pump–thaw cycles, and stored over activated 3 Å molecular sieves. Mass spectrometry analyses were performed on an Advion ExpressionL compact mass spectrometer equipped with an electrospray probe and an ion-trap mass analyzer. Direct injection analysis was employed in all cases with a sample solution in acetonitrile. Elemental analyses were performed on a PerkinElmer 2400 series II analyzer at the CENTC Elemental Analysis Facility, University of Rochester.

Cyclic voltammetry experiments were recorded with a Bio-Logic SP-150 potentiostat at scan rate of 50, 100, 200 and 400 mV s^{−1}. All measurements were performed in a dinitrogen-filled glovebox using a three-electrode cell configuration that consisted of a glassy carbon (Ø = 3.0 mm) working electrode, a platinum wire counter electrode, and a silver wire pseudo-reference electrode. A 0.1 M [⁷Bu₄N][PF₆] solution in dry acetonitrile was used as the electrolyte solution. All redox events were referenced using the ferrocenium/ferrocene (Fc⁺/Fc) redox couple (0.40 V vs. SCE).⁵²

Synthesis of [1,1'-biphenyl]-2-yltrichlorosilane

A 1.6 M solution of *n*-butyllithium in hexane (1.1 eq., 62.0 mL) was slowly added to a stirred solution of 2-bromo-1,1'-biphenyl

(21.0 g, 1.0 eq., 90.0 mmol) in anhydrous diethyl ether (100 mL) at −78 °C. After 5 h, the reaction mixture was added to a solution of silicon tetrachloride (3.0 eq., 270 mol, 45.9 g) in anhydrous diethyl ether (100 mL) at −78 °C. The stirred mixture was allowed to warm up to room temperature over 3 h. Subsequently, precipitated byproducts were filtered off under nitrogen. The product was isolated from the filtered solution by distillation under reduced pressure as a colorless solid (13.2 g, 51%).

¹H NMR (CD₃Cl, 400 MHz) δ = 8.12 (dd, *J* = 8, 1 Hz, 1H), 7.66 (td, *J* = 8, 1 Hz, 1H), 7.55 (td, *J* = 8, 1 Hz, 1H), 7.50–7.41 (m, 6H); ¹³C{¹H} NMR (CDCl₃, 101 MHz) δ 149.18, 141.62, 135.32, 132.61, 131.10, 129.74, 128.27, 128.23, 127.04.

General procedure for the synthesis of organosilyl-functionalized POT, THA₃[PW₉O₃₄(RSiOH)₃]

K₉[PW₉O₃₄]·16H₂O (1.0 eq., 2.5 g, 0.87 mmol) and tetra-*n*-hexylammonium bromide (4.0 eq., 1.5 g, 3.48 mmol) were placed in oven-dried 100 mL round-bottomed flask. Then, anhydrous acetonitrile (30 mL) was added and the stirred suspension was cooled in an ice/NaCl_(aq.) bath under positive pressure of argon. The desired trichlorosilane derivative (3.0 eq., 2.6 mmol) was then added to the cold mixture and the stirred suspension allowed to warm up to room temperature overnight. Subsequently, white solids were filtered, and acetonitrile was removed from the filtrate under reduced pressure. The gummy residue was suspended in approx. 20 mL of ethanol, filtered on a fine porosity frit, washed with ethanol (10 mL) and diethyl ether (10 mL) and finally air dried. The final product, THA₃[PW₉O₃₄(RSiOH)₃], was obtained as a white powder.

Compound 1. THA₃[PW₉O₃₄(^tBuSiOH)₃]: 2.99 g, 89%

¹H NMR (400 MHz, CD₃CN) δ 4.91 (s, 3H, Si–OH), 3.09 (m, 24H, THA N–CH₂–), 1.61 (m, 24H, THA N–CH₂–CH₂–), 1.34 (s, 72H, THA –CH₂–(CH₂)₃–CH₃), 1.00 (s, 27H, Si–C(CH₃)₃), 0.91 (t, *J* = 6.4 Hz, 36H, THA –CH₃); ³¹P{¹H} NMR (162 MHz, CD₃CN) δ −15.76. Spectra matching previous report.³⁰ ESI-MS (–)ve found: 845.1, calc. 845.5.

Compound 2. THA₃[PW₉O₃₄(PhSiOH)₃]: 2.85 g, 89%

¹H NMR (400 MHz, CD₃CN) δ 7.72 (d, 6H, Si–C₆H₅), 7.42 (m, 9H, Si–C₆H₅), 5.59 (s, 3H, Si–OH), 3.09 (m, 24H, THA N–CH₂–), 1.61 (m, 24H, THA N–CH₂–CH₂–), 1.34 (s, 72H, THA –CH₂–(CH₂)₃–CH₃), 0.91 (t, *J* = 6.4 Hz, 36H, THA –CH₃); ³¹P{¹H} NMR (162 MHz, CD₃CN) δ −15.77; elemental analysis: calc. for THA₃[PW₉O₃₄(PhSiOH)₃]·2H₂O 29.25 (% C), 4.85 (% H), 1.14 (% N); found 28.94 (% C), 4.55 (% H), 1.13 (% N); ESI-MS (–)ve found: 865.4, calc. 865.5.

Compound 3. THA₃[PW₉O₃₄(CySiOH)₃]: 2.66 g, 83%

¹H NMR (400 MHz, CD₃CN) δ 4.90 (s, 3H, Si–OH), 3.10 (m, 24H, THA N–CH₂–), 1.76 (m, 12H, Si–Cy), 1.62 (m, 3H from Si–Cy overlapping with 24H from THA N–CH₂–CH₂–), 1.40–1.23 (m, 15H from Si–Cy overlapping with 72H from THA –CH₂–(CH₂)₃–CH₃), 0.91 (t, *J* = 6.5 Hz, 36H, THA –CH₃), 0.79 (t, *J* = 9.4 Hz, 3H, CH₃–Si); ³¹P{¹H} NMR (162 MHz, CD₃CN) δ −15.76; elemental analysis: calc. for THA₃[PW₉O₃₄(CySiOH)₃] 29.39 (% C), 4.85 (% H), 1.14 (% N); found 28.94 (% C), 4.55 (% H), 1.13 (% N); ESI-MS (–)ve found: 865.4, calc. 865.5.

C), 5.26 (% H), 1.14 (% N); found 29.20 (% C), 5.12 (% H), 1.13 (% N); ESI-MS (–)ve found: 871.2, calc. 871.5.

Compound 4. $\text{THA}_3[\text{PW}_9\text{O}_{34}(\text{PhPhSiOH})_3]$: 3.20 g, 94%

^1H NMR (400 MHz, CD_3CN) δ 7.91 (d, J = 6.9 Hz, 3H, Si-PhPh), 7.54 (td, J = 7.4, 1.2 Hz, 3H, Si-PhPh), 7.50–7.42 (m, 9H, Si-PhPh), 7.38 (d, J = 7.4 Hz, 3H, Si-PhPh), 7.14 (t, J = 7.7 Hz, 6H, Si-PhPh), 6.56 (t, J = 7.4 Hz, 3H, Si-PhPh), 4.70 (s, 3H, Si-OH), 3.09 (m, 24H, THA N-CH₂–), 1.61 (m, 24H, THA N-CH₂–CH₂–), 1.34 (s, 72H, THA –CH₂–(CH₂)₃–CH₃), 0.91 (t, J = 6.4 Hz, 36H, THA –CH₃); $^{31}\text{P}\{^1\text{H}\}$ NMR (162 MHz, CD_3CN) δ –15.99. Calc. for $\text{THA}_3[\text{PW}_9\text{O}_{34}(\text{PhPhSiOH})_3]$ 33.36 (% C), 4.82 (% H), 1.08 (% N); found 33.26 (% C), 4.72 (% H), 1.07 (% N); ESI-MS (–)ve found: 941.5, calc. 941.5.

Drying procedure for the organosilyl-functionalized POT, $\text{THA}_3[\text{PW}_9\text{O}_{34}(\text{RSiOH})_3]$

The white solid obtained previously is charged in a 50 mL air-free round bottom flask and placed under vacuum on the Schlenk line. Using an oil bath, the flask is heated to 210 °C and maintained at this temperature for 4 h, under dynamic vacuum. The flask is then closed and transferred in the glovebox.

CAUTION: Not every oil used for a bath is suitable for heating at such high temperature and the actual range of temperature accessible for the oil should be checked using the information provided by the supplier.

General procedure for the synthesis of the hafnium complexes, $\text{THA}_3[\text{PW}_9\text{O}_{34}(\text{RSiO})_3\text{Hf}(\text{O}^t\text{Bu})]$

Hafnium *tert*-butoxide (1.2 eq.) was added to a solution of the suitably dried ligand $\text{THA}_3[\text{PW}_9\text{O}_{34}(\text{RSiOH})_3]$ (1.0 eq., 200 mg) in tetrahydrofuran (4 mL). The colorless solution was stirred at room temperature (the reaction time varied: 1 h for 5–7 and 16 to 24 h for 8). Removal of volatiles under reduced pressure yielded a white solid which was washed twice with 5 mL of Et₂O and dried under vacuum.

Complex 5. $\text{THA}_3[\text{PW}_9\text{O}_{34}(\text{tBuSiO})_3\text{Hf}(\text{O}^t\text{Bu})]$: 180 mg, 84%

^1H NMR (400 MHz, CD_3CN) δ 3.09 (m, 24H, THA N-CH₂–), 1.61 (m, 24H, THA N-CH₂–CH₂–), 1.34 (s, 72H, THA –CH₂–(CH₂)₃–CH₃), 1.25 (s, 9H, Hf-OC(CH₃)₃), 1.04 (s, 27H, Si-C(CH₃)₃), 0.91 (t, J = 6.4 Hz, 36H, THA –CH₃); $^{31}\text{P}\{^1\text{H}\}$ NMR (162 MHz, CD_3CN) δ –16.19; calc. for $\text{THA}_3[\text{PW}_9\text{O}_{34}(\text{tBuSiO})_3\text{Hf}(\text{O}^t\text{Bu})]$ 29.39 (% C), 5.26 (% H), 1.14 (% N); found 29.20 (% C), 5.12 (% H), 1.13 (% N).

Complex 6. $\text{THA}_3[\text{PW}_9\text{O}_{34}(\text{PhSiO})_3\text{Hf}(\text{O}^t\text{Bu})]$: 190 mg, 89%

^1H NMR (400 MHz, CD_3CN) δ 7.79 (m, 6H, Si-C₆H₅), 7.37 (m, 9H, Si-C₆H₅), 3.10 (m, 24H, THA N-CH₂–), 1.61 (m, 24H, THA N-CH₂–CH₂–), 1.34 (s, 72H, THA –CH₂–(CH₂)₃–CH₃), 1.10 (s, 9H, Hf-OC(CH₃)₃), 0.91 (t, J = 6.4 Hz, 36H, THA –CH₃); $^{31}\text{P}\{^1\text{H}\}$ NMR (162 MHz, CD_3CN) δ –16.17; calc. for $\text{THA}_3[\text{PW}_9\text{O}_{34}(\text{PhSiO})_3\text{Hf}(\text{O}^t\text{Bu})]$ 28.88 (% C), 4.64 (% H), 1.08 (% N); found 28.62 (% C), 4.31 (% H), 0.95 (% N).

Complex 7. $\text{THA}_3[\text{PW}_9\text{O}_{34}(\text{CySiO})_3\text{Hf}(\text{O}^t\text{Bu})]$: 187 mg, 88%

^1H NMR (400 MHz, CD_3CN) δ 3.10 (m, 24H, THA N-CH₂–), 1.89 (d, J = 12 Hz, 6H, Si-Cy), 1.76 (d, J = 11 Hz, 6H, Si-Cy), 1.62 (m, 3H from Si-Cy overlapping with 24H from THA N-CH₂–CH₂–), 1.40–1.24 (m, 15H from Si-Cy overlapping with

72H from THA –CH₂–(CH₂)₃–CH₃), 1.23 (s, 9H, Hf-OC(CH₃)₃), 0.91 (t, J = 6.5 Hz, 36H, THA –CH₃), 0.71 (t, J = 12 Hz, 3H, CH–Si); $^{31}\text{P}\{^1\text{H}\}$ NMR (162 MHz, CD_3CN) δ –16.40; calc. for $\text{THA}_3[\text{PW}_9\text{O}_{34}(\text{CySiO})_3\text{Hf}(\text{O}^t\text{Bu})_{0.9}(\text{OH})_{0.1}]$ (partially hydrolyzed) 28.67 (% C), 5.07 (% H), 1.07 (% N); found 28.29 (% C), 4.90 (% H), 0.95 (% N).

Complex 8. $\text{THA}_3[\text{PW}_9\text{O}_{34}(\text{PhPhSiO})_3\text{Hf}(\text{O}^t\text{Bu})]$: 197 mg, 93%

^1H NMR (400 MHz, CD_3CN) δ 8.17 (d, J = 7 Hz, 3H, Si-PhPh), 7.57 (d, J = 7 Hz, 6H, Si-PhPh), 7.47–7.33 (m, 12H, Si-PhPh), 7.29 (m, 6H, Si-PhPh), 3.09 (m, 24H, THA N-CH₂–), 1.61 (m, 24H, THA N-CH₂–CH₂–), 1.34 (s, 72H, THA –CH₂–(CH₂)₃–CH₃), 1.13 (s, 9H, Hf-OC(CH₃)₃), 0.91 (t, J = 6.4 Hz, 36H, THA –CH₃); $^{31}\text{P}\{^1\text{H}\}$ NMR (162 MHz, CD_3CN) δ –15.67. Calc. for $\text{THA}_3[\text{PW}_9\text{O}_{34}(\text{PhPhSiO})_3\text{Hf}(\text{O}^t\text{Bu})]$ 32.52 (% C), 4.68 (% H), 1.02 (% N); found 32.37 (% C), 4.59 (% H), 1.34 (% N).

Characterization of the hydrolyzed species

In the presence of trace amounts of water, the hafnium complexes 5–8 undergo hydrolysis of the Hf-alkoxide bond, resulting in hydroxo compounds (potentially dimeric – see text).

Hydrolyzed form of complex 5. $\text{THA}_3[\text{PW}_9\text{O}_{34}(\text{tBuSiO})_3\text{Hf}(\text{OH})]$: ^1H NMR (400 MHz, CD_3CN) δ 3.72 (s, 1H, Hf–OH), 3.12 (m, 24H, THA N-CH₂–), 1.63 (m, 24H, THA N-CH₂–CH₂–), 1.34 (s, 72H, THA –CH₂–(CH₂)₃–CH₃), 1.01 (s, 27H, Si-C(CH₃)₃), 0.91 (t, J = 6.4 Hz, 36H, THA –CH₃); $^{31}\text{P}\{^1\text{H}\}$ NMR (162 MHz, CD_3CN) δ –16.40; ESI-MS (–)ve found: 909.1, calc. 908.8.

Hydrolyzed form of complex 6. $\text{THA}_3[\text{PW}_9\text{O}_{34}(\text{PhSiO})_3\text{Hf}(\text{OH})]$: ^1H NMR (400 MHz, CD_3CN) δ 7.61 (d, J = 8 Hz, 6H, Si-C₆H₅), 7.37 (t, J = 7 Hz, 3H, Si-C₆H₅), 7.28 (t, J = 7 Hz, 6H, Si-C₆H₅), 4.77 (s, 1H, Hf–OH), 3.10 (m, 24H, THA N-CH₂–), 1.61 (m, 24H, THA N-CH₂–CH₂–), 1.34 (s, 72H, THA –CH₂–(CH₂)₃–CH₃), 1.10 (s, 9H, Hf-OC(CH₃)₃), 0.91 (t, J = 6.4 Hz, 36H, THA –CH₃); $^{31}\text{P}\{^1\text{H}\}$ NMR (162 MHz, CD_3CN) δ –16.13; ESI-MS (–)ve found: 929.8, calc. 929.5.

Hydrolyzed form of complex 7. $\text{THA}_3[\text{PW}_9\text{O}_{34}(\text{CySiO})_3\text{Hf}(\text{OH})]$: ^1H NMR (400 MHz, CD_3CN) δ 4.39 (s, 1H, Hf–OH), 3.10 (m, 24H, THA N-CH₂–), 1.89 (d, J = 12 Hz, 6H, Si-Cy), 1.76 (d, J = 11 Hz, 6H, Si-Cy), 1.62 (m, 3H from Si-Cy overlapping with 24H from THA N-CH₂–CH₂–), 1.40–1.24 (m, 15H from Si-Cy overlapping with 72H from THA –CH₂–(CH₂)₃–CH₃), 0.91 (m, 3H from Si-Cy overlapping with 36H, from THA –CH₃); $^{31}\text{P}\{^1\text{H}\}$ NMR (162 MHz, CD_3CN) δ –16.47; ESI-MS (–)ve found: 936.0, calc. 935.5.

Hydrolyzed form of complex 8. $\text{THA}_3[\text{PW}_9\text{O}_{34}(\text{PhPhSiO})_3\text{Hf}(\text{OH})]$: ^1H NMR (400 MHz, CD_3CN) δ 7.83 (d, J = 7 Hz, 3H, Si-PhPh), 7.38 (d, J = 8 Hz, 6H, Si-PhPh), 7.29 (t, J = 8 Hz, 9H, Si-PhPh), 7.18 (m, 6H, Si-PhPh), 7.04 (d, J = 8 Hz, 3H, Si-PhPh), 3.96 (s, 1H, Hf–OH), 3.09 (m, 24H, THA N-CH₂–), 1.61 (m, 24H, THA N-CH₂–CH₂–), 1.34 (s, 72H, THA –CH₂–(CH₂)₃–CH₃), 0.91 (t, J = 6.4 Hz, 36H, THA –CH₃); $^{31}\text{P}\{^1\text{H}\}$ NMR (162 MHz, CD_3CN) δ –16.04; ESI-MS (–)ve found: 1006.0, calc. 1006.2.

Conflicts of interest

There are no conflicts to declare.

Acknowledgements

This work is supported by the U.S. Department of Energy, Office of Science, Office of Basic Energy Sciences Heavy Element Program, under award DE-SC0020436. O. N. thanks the Alexander von Humboldt foundation for a Feodor Lynen Research Fellowship. The authors would like to acknowledge Dr Geoffroy Guillemot for fruitful discussions and generous advice during the composition of this manuscript.

Notes and references

- 1 P. Serna and B. C. Gates, *Acc. Chem. Res.*, 2014, **47**, 2612–2620.
- 2 T. J. Marks, *Acc. Chem. Res.*, 2002, **25**, 57–65.
- 3 T. Maschmeyer, F. Rey, G. Sankar and J. M. Thomas, *Nature*, 1995, **378**, 159–162.
- 4 C. Coperet, A. Comas-Vives, M. P. Conley, D. P. Estes, A. Fedorov, V. Mougel, H. Nage, F. Nunez-Zarur and P. A. Zhizhko, *Chem. Rev.*, 2016, **116**, 323–421.
- 5 D. B. Cordes, P. D. Lickiss and F. Rataboul, *Chem. Rev.*, 2010, **110**, 2081–2173.
- 6 S. Garg, D. K. Unruh and C. Krempner, *Catal. Sci. Technol.*, 2021, **11**, 211–218.
- 7 *Polyoxometalate Chemistry From Topology via Self-Assembly to Applications*, ed. M. T. Pope and A. Muller, Kluwer Academic Publishers, 2002.
- 8 B. E. Petel, R. L. Meyer, M. L. Maiola, W. W. Brennessel, A. M. Muller and E. M. Matson, *J. Am. Chem. Soc.*, 2020, **142**, 1049–1056.
- 9 V. W. Day and W. G. Klemperer, *Mol. Eng.*, 1993, **3**, 61–78.
- 10 V. W. Day, C. W. Earley, W. G. Klemperer and D. J. Maltbie, *J. Am. Chem. Soc.*, 1985, **107**, 8261–8262.
- 11 E. V. Radkov, V. G. Young and R. H. Beer, *J. Am. Chem. Soc.*, 1999, **121**, 8953–8954.
- 12 G. Hervé, A. Tézé and R. Contant, in *Polyoxometalate Molecular Science*, ed. J. J. Borrás-Almenar, E. Coronado, A. Müller and M. Pope, Springer Netherlands, Dordrecht, 2003, pp. 33–54.
- 13 R. J. Errington, S. S. Petkar, P. S. Middleton, W. McFarlane, W. Clegg, R. A. Coxall and R. W. Harrington, *Dalton Trans.*, 2007, 5211–5222.
- 14 P. Putaj and F. Lefebvre, *Coord. Chem. Rev.*, 2011, **255**, 1642–1685.
- 15 R. L. Meyer, W. W. Brennessel and E. M. Matson, *Polyhedron*, 2018, **156**, 303–311.
- 16 R. K. C. Ho and W. G. Klemperer, *J. Am. Chem. Soc.*, 1978, **100**, 6772–6774.
- 17 A. M. Khenkin and R. Neumann, *Angew. Chem., Int. Ed.*, 2000, **39**, 4088–4090.
- 18 B. E. Petel and E. M. Matson, *Chem. Commun.*, 2020, **56**, 13477–13490.
- 19 A. Proust, B. Matt, R. Villanneau, G. Guillemot, P. Gouzerh and G. Izzet, *Chem. Soc. Rev.*, 2012, **41**, 7605–7622.
- 20 A. V. Anyushin, A. Kondinski and T. N. Parac-Vogt, *Chem. Soc. Rev.*, 2020, **49**, 382–432.
- 21 T. Minato, K. Suzuki, K. Yamaguchi and N. Mizuno, *Chem. – Eur. J.*, 2017, **23**, 14213–14220.
- 22 L. E. VanGelder, W. W. Brennessel and E. M. Matson, *Polyhedron*, 2019, **167**, 119–126.
- 23 A. Mazeaud, N. Ammari, F. Robert and R. Thouvenot, *Angew. Chem., Int. Ed. Engl.*, 1996, **35**, 1961–1964.
- 24 G. Guillemot, E. Matricardi, L.-M. Chamoreau, R. Thouvenot and A. Proust, *ACS Catal.*, 2015, **5**, 7415–7423.
- 25 C. R. Mayer and R. Thouvenot, *J. Chem. Soc., Dalton Trans.*, 1998, 7–14.
- 26 R. Villanneau, A. B. Djamâa, L.-M. Chamoreau, G. Gontard and A. Proust, *Eur. J. Inorg. Chem.*, 2013, **2013**, 1815–1820.
- 27 S. Bareyt, S. Piligkos, B. Hasenknopf, P. Gouzerh, E. Lacote, S. Thorimbert and M. Malacria, *J. Am. Chem. Soc.*, 2005, **127**, 6788–6794.
- 28 A. J. Kibler and G. N. Newton, *Polyhedron*, 2018, **154**, 1–20.
- 29 M. Boujtita, J. Boixel, E. Blart, C. R. Mayer and F. Odobel, *Polyhedron*, 2008, **27**, 688–692.
- 30 T. Zhang, L. Mazaud, L.-M. Chamoreau, C. Paris, A. Proust and G. Guillemot, *ACS Catal.*, 2018, **8**, 2330–2342.
- 31 T. Zhang, A. Solé-Daura, S. Hostachy, S. Blanchard, C. Paris, Y. Li, J. J. Carbo, J. M. Poblet, A. Proust and G. Guillemot, *J. Am. Chem. Soc.*, 2018, **140**, 14903–14914.
- 32 T. Zhang, A. Solé-Daura, H. Fouilloux, J. M. Poblet, A. Proust, J. J. Carbó and G. Guillemot, *ChemCatChem*, 2021, **13**, 1220–1229.
- 33 A. Solé-Daura, T. Zhang, H. Fouilloux, C. Robert, C. M. Thomas, L.-M. Chamoreau, J. J. Carbó, A. Proust, G. Guillemot and J. M. Poblet, *ACS Catal.*, 2020, **10**, 4737–4750.
- 34 R. D. Shannon, *Acta Crystallogr., Sect. A: Cryst. Phys., Diffraction, Theor. Gen. Crystallogr.*, 1976, **32**, 751–767.
- 35 R. Contant, *Can. J. Chem.*, 1987, **65**, 568–573.
- 36 B. D. Shepherd, D. R. Powell and R. West, *Organometallics*, 1989, **8**, 2664–2669.
- 37 A. Misra, K. Kozma, C. Streb and M. Nyman, *Angew. Chem.*, 2020, **59**, 596–612.
- 38 J. J. Walsh, A. M. Bond, R. J. Forster and T. E. Keyes, *Coord. Chem. Rev.*, 2016, **306**, 217–234.
- 39 D. Agustin, J. Dallery, C. Coelho, A. Proust and R. Thouvenot, *J. Organomet. Chem.*, 2007, **692**, 746–754.
- 40 V. Duffort, R. Thouvenot, C. Afonso, G. Izzet and A. Proust, *Chem. Commun.*, 2009, 6062–6064.
- 41 A. Al-Yasari, N. Van Steerteghem, H. Kearns, H. El Moll, K. Faulds, J. A. Wright, B. S. Brunshwig, K. Clays and J. Fielden, *Inorg. Chem.*, 2017, **56**, 10181–10194.
- 42 Q. Chen, D. P. Goshorn, C. P. Scholes, X. L. Tan and J. Zubieta, *J. Am. Chem. Soc.*, 1992, **114**, 4667–4681.
- 43 N. Joo, S. Renaudineau, G. Delapierre, G. Bidan, L. M. Chamoreau, R. Thouvenot, P. Gouzerh and A. Proust, *Chem. – Eur. J.*, 2010, **16**, 5043–5051.
- 44 P. A. Aparicio, J. M. Poblet and X. López, *Eur. J. Inorg. Chem.*, 2013, **2013**, 1910–1916.

- 45 S. Fujimoto, J. M. Cameron, R. J. Wei, K. Kastner, D. Robinson, V. Sans, G. N. Newton and H. Oshio, *Inorg. Chem.*, 2017, **56**, 12169–12177.
- 46 J. M. Cameron, S. Fujimoto, R. J. Wei, G. N. Newton and H. Oshio, *Dalton Trans.*, 2018, **47**, 10590–10594.
- 47 C. Boglio, K. Micoine, P. Remy, B. Hasenknopf, S. Thorimbert, E. Lacote, M. Malacria, C. Afonso and J. C. Tabet, *Chem. – Eur. J.*, 2007, **13**, 5426–5432.
- 48 K. Nomiya, K. Ohta, Y. Sakai, T.-a. Hosoya, A. Ohtake, A. Takakura and S. Matsunaga, *Bull. Chem. Soc. Jpn.*, 2013, **86**, 800–812.
- 49 F. de Azambuja and T. N. Parac-Vogt, *ACS Catal.*, 2019, **9**, 10245–10252.
- 50 L. Vandebroek, E. De Zitter, H. G. T. Ly, D. Conic, T. Mihaylov, A. Sap, P. Proost, K. Pierloot, L. Van Meervelt and T. N. Parac-Vogt, *Chem. – Eur. J.*, 2018, **24**, 10099–10108.
- 51 T. J. Boyle, L. A. Steele, P. D. Burton, S. M. Hoppe, C. Lockhart and M. A. Rodriguez, *Inorg. Chem.*, 2012, **51**, 12075–12092.
- 52 N. G. Connelly and W. E. Geiger, *Chem. Rev.*, 1996, **96**, 877–910.